LRP 771/03 October 2003

Papers presented at the 14th International Stellarator Workshop

September 22-26, 2003
Greifswald, Germany

Available in colour on the web at
http://crppwww/conferences/

ISSN 0458-5895

LIST OF CONTENTS

MHD STABILITY OF FREE BOUNDARY QUASIAXISYMMETRIC STELLARATOR EQUILIBRIA WITH FINITE BOOTSTRAP CURRENT

W.A. Cooper [1], S. Ferrando i Margalet S.J. Allfrey [1], J. Kisslinger[2], H. Wobig[2], Y. Narushima[3], S. Okamura[3], C. Suzuki[3], K. Y. Watanabe[3], K. Yamazaki[3], M. Yu. Isaev,[4]

[1] Centre de Recherches en Physique des Plasmas, Association Euratom-Confédération Suisse, Ecole Polytechnique Fédérale de Lausanne, Switzerland

[2] Max-Plank-Institut für Plasmaphysik, IPP-EURATOM Association, Germany

[3] National Institute for Fusion Science, Oroshi-cho 322-6, Toki 509-5292, Japan

[4] Russian Research Centre "Kurchatov Institute", Moscow, Russia

1 Introduction

Interest in quasiaxisymmetric stellarator (QAS) [1, 2] systems has been sparked by the realisation that though the devices are three dimensional (3D), the magnetic field strength B spectrum is dominated by a $m = 1, n = 0$ component. Consequently, the behaviour of the guiding centre drift orbits which depends only on B in Boozer magnetic coordinates [3] should be very similar to that in a tokamak. Further advantages perceived are compact aspect ratio, typically less than 4 and no need for Ohmic current so the system is inherently steady state. However, this type of device can exhibit a large bootstrap current (BC) at finite β which increases the rotational transform as in tokamaks. This can cause low order resonant surfaces to appear at the edge of the plasma and provide free energy to drive global external kink modes. The NCSX and CHS-qa Experimental concepts to test the physics properties of quasiaxisymmetry have been proposed at PPPL [4] and NIFS [5], respectively. The optimisation of such systems have included neoclassical transport, α-particle confinement and MHD stability with finite BC. Specific studies with respect to the effect of the BC on MHD stability have been carried out previously for fixed boundary equilibria [6, 7]. In this work, we address the impact of the BC on equilibrium and stability of a 2 field period QAS reactor system when the plasma boundary is free.

2 The Bootstrap Current Model

The bootstrap current model that we apply is based on a quasianalytic formulation valid in the collisionless $1/\nu$ regime that is succinctly described by *Johnson et al.* [8] and is based on previous derivations presented in references therein. The set of equations used to obtain the BC in the $1/\nu$ regime are

$$
\begin{aligned}
2\pi J(s) &= 2\pi \int_0^s ds \frac{< \boldsymbol{j} \cdot \boldsymbol{B} >}{< B^2 >} \Phi'(s) \\
< \boldsymbol{j} \cdot \boldsymbol{B} > &= -G_b \Big(L_1 \frac{dp}{d\Phi} + L_2 \rho \frac{dT}{d\Phi} \Big)
\end{aligned}
$$

$$
\begin{aligned}
G_b(s) &= \frac{1}{f_t}\left[< g_2 > - \frac{3 < B^2 >}{4B_{max}^2} \int_0^1 d\lambda \lambda \frac{< g_4 >}{< g_1 >}\right] \\
f_t &= 1 - \frac{3 < B^2 >}{4B_{max}^2} \int_0^1 d\lambda \frac{\lambda}{< g_1 >} \\
g_1 &= \sqrt{(1 - \lambda B / B_{max})} \\
\boldsymbol{B} \cdot \boldsymbol{\nabla}(g_2/B^2) &= \boldsymbol{B} \times \boldsymbol{\nabla}\Phi \cdot \boldsymbol{\nabla} B^{-2} \\
\boldsymbol{B} \cdot \boldsymbol{\nabla}(g_4/g_1) &= \boldsymbol{B} \times \boldsymbol{\nabla}\Phi \cdot \boldsymbol{\nabla} g_1^{-1} \\
g2(B_{max}) &= g4(B_{max}) = 0.
\end{aligned}
$$

The toroidal current profile that must be provided to the VMEC code is $2\pi J(s)$. The averaged BC on each surface $< \boldsymbol{j} \cdot \boldsymbol{B} >$ is proportional to the geometric factor G_b, viscosity coefficients L_1 and L_2 found in Ref. [8] and references therein and derivatives of the pressure and temperature with respect to the toroidal magnetic flux function Φ. The geometric factor depends on the trapped particle fraction f_t and the integration of flux surface average functions with respect to the pitch angle λ. The BC in the $1/\nu$ limit is determined by two coupled ordinary differential equations (ODE) along the B-field lines which are solved using a Fourier technique on each flux surface for each pitch angle.

3 The Resonance Detuning Model

The inversion of the $\boldsymbol{B} \cdot \boldsymbol{\nabla}$ operator to obtain expressions for the geometric factor components g_2 and g_4/g_1 will diverge at mode rational surfaces and this can produce artificial discontinuities in the BC profile. The singular term from the $\boldsymbol{B} \cdot \boldsymbol{\nabla}$ operator inversion has the form $[m\psi'(s) - n\Phi'(s)]^{-1}$ in Boozer magnetic coordinates [3] To resolve this singularity, we replace it with [9] $[m\psi'(s) - n\Phi'(s)]/\{[m\psi'(s) - n\Phi'(s)]^2 + \Delta_m^2\}$. We specifically choose $\Delta_m = [(m+1)\psi'(s) - n\Phi'(s)]\Delta$, where m is the poloidal mode number, n is the toroidal mode number, ψ is the poloidal magnetic flux function and prime ($'$) indicates the derivative of a flux surface quantity with respect to s. Then the parameter Δ^2 that controls the detuning becomes dimensionless and can therefore be applied to any plasma confinement system regardless of size or B-field strength.

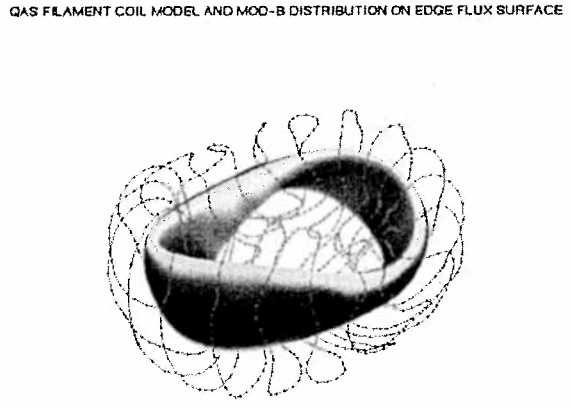

Fig. 1. The filamentary coil model of a 2-period QAS reactor device and the mod-B structure of the plasma-vacuum interface boundary computed with the VMEC code.

4 Magnetohydrodynamic Equilibria

The free boundary version of the VMEC equilibrium code [10] is applied to investigate the effects of the bootstrap current on the plasma shape, rotational transform and other properties. Vacuum magnetic fields are computed using the Biot-Savart Law from currents of a coil system that has been optimised to obtain a 2-field period QAS reactor system. The pressure profile chosen in this study as input for VMEC has the form $p(s) = p(0)[1 - s - 0.1(1 - s^{10})]/0.9$ that is nearly parabolic but with vanishing gradient at the edge. The other profile that is required as input is the toroidal plasma curent $2\pi J(s)$ which we obtain by iterating between equilibrium calculations and BC calculations until a converged profile is achieved. A module of the TERPSICHORE code [11] has been adapted to compute the BC in the $1/\nu$ limit that solves the ODE's described in Section 2 in a Boozer coordinate frame. The filaments and the mod-B contours on the outermost flux surface computed with the VMEC code are displayed in Fig. 1.

5 Self Consistent MHD Equilibria with Finite Bootstrap Current

Successive calculations of VMEC equilibria and the bootstrap current typically take between $8 - 20$ iterations to converge a current profile. In Fig. 2, we show the BC profile at $\beta = 1.77\%$ for values of the resonance detuning parameter Δ^2 of 10^{-4}, 10^{-3} and 10^{-2}. For $\Delta^2 = 10^{-4}$, the profile exhibits sharp discontinuities at rational surfaces. These tend to disappear for $\Delta^2 = 10^{-3}$, though the BC profile retains step-like features. For $\Delta^2 = 10^{-2}$, the profile becomes completely smooth. The integrated BC is virtually the same for all these values of Δ^2. In Fig. 3, we display the converged BC profiles for several values of β. For $\beta > 3\%$, a larger value of Δ^2 is required to converge the BC profile. At the highest $\beta = 3.78\%$ achieved, a magnitude of $\Delta^2 = 5.22 \times 10^{-2}$ is required and the integrated current achieved was significantly smaller than that in the range $\beta = 3.25 - 3.5\%$. The converged profile may have been achieved by supressing the current near the edge. For $\beta > 4\%$, we were unable to compute a converged BC profile unlike the conditions previously treated with fixed boundary QAS calculations where we were able to attain converged BC at $\beta > 5\%$ [7]. This can be attributed to the fact that not only the BC profile but also the plasma shape and column position is varying form one iteration to the next. The change

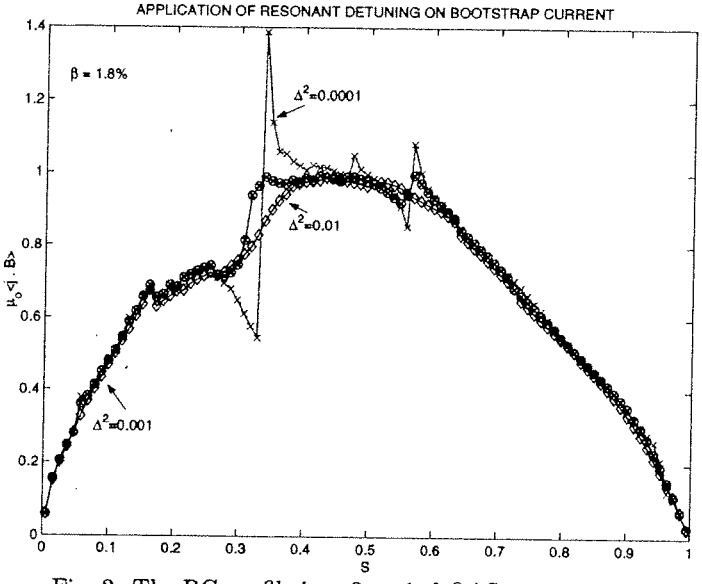

Fig. 2. The BC profile in a 2-period QAS reactor with different values of the resonance detuning parameter Δ^2.

of shape and position of the plasma column with finite β and BC is illustrated in Fig. 4. As β is increased from 0 to 3.25% with the BC set to zero, the plasma column exhibits a noticeable outward radial displacement bringing it closer to the coils. When the self consistent BC is included at $\beta = 3.25\%$, the outer edge of the vertically elongated up-down symmetric cross section does not move. However, the BC causes the plasma shape to become more elongated regardless of cross section. Furthermore, the horizontally elongated up-down symmetric cross section becomes distorted into a bomblet shape. An analysis of the spectrum of the B-field strength shows that the dominant component is $m = 1, n = 0$ as would be expected in a QAS system (Fig. 5). The distribution of mod-B near the edge in Boozer magnetic coordinates shows that higher order components play an important role. When the boundary flux surface is unwrapped, closed mod-B contours are observed near the regions of minimum-B at the outer edge and maximum-B on the inner edge. These effects are displayed in Fig. 6. For $\beta > 3\%$, the converged BC profile exhibits discontinuous jumps which are not associated with resonant effects at mode rational surfaces. These discontinuities are correlated with jumps in the locations of the maxima of B on adjacent flux surfaces. This is shown in Figs. 7 and 8 where the mod-B distribution is displayed on surfaces with $s = 84.5/96$ and $s = 85.5/96$ which have been unwrapped and plotted as a function of the Boozer poloidal and toroidal angular variables θ and ϕ, respectively. The positions of the B-maxima are indicated with the symbol '$*$' in Figs. 6-8.

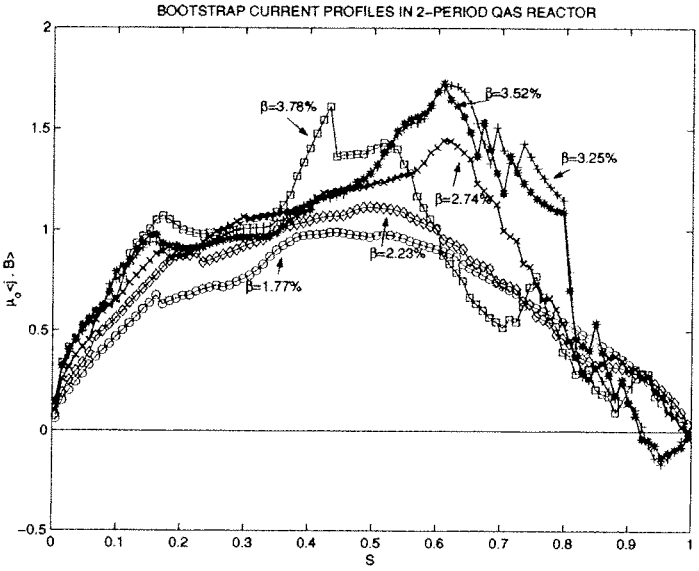

Fig. 3. The BC profiles for different values of β.

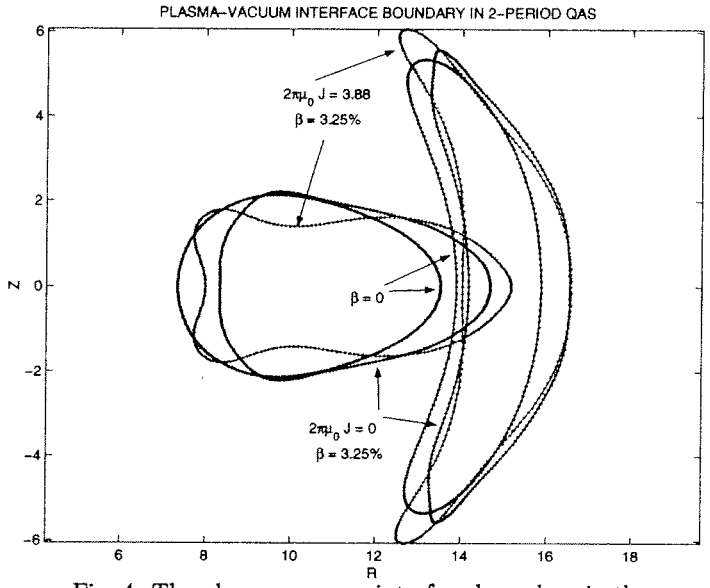

Fig. 4. The plasma-vacuum interface boundary in the vacuum state and at $\beta = 3.25\%$ with and without the BC effect.

6 Ideal MHD Stability Properties

The impact of the BC on the ideal MHD stability properties of a 2-period QAS reactor system is investigated with the TERPSICHORE code [11]. A pseudoplasma treatment of the vacuum is considered and therefore a conducting wall that approaches conformal conditions is prescribed. The pressure profile and the rotational transform profile obtained with self consistent BC is presented in Fig. 9. The most unstable eigenvalue is plotted in Fig. 10 as a function of β which shows a marginal point at $\beta \simeq 1.8\%$. For $\beta > 1.8\%$, the BC causes the critical $\iota = 1/2$ resonant surface to appear in the plasma. The system then becomes susceptible to $m/n = 2/1$ external kink destabilisation driven by the free energy provided by the BC. The five leading Fourier terms of the radial component of the displacement vector are displayed in Fig. 11 at $\beta = 2.25\%$. This shows that the mode is indeed dominated by a $m/n = 2/1$ component which increases radially towards the edge of the plasma that is a characteristic feature of an external kink.

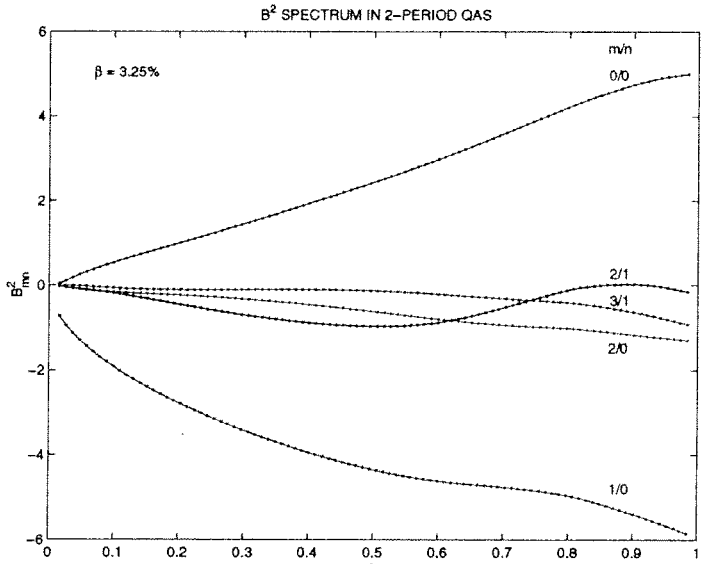

Fig. 5. The leading components of the B^2 spectrum at $\beta = 3.25\%$ with finite BC.

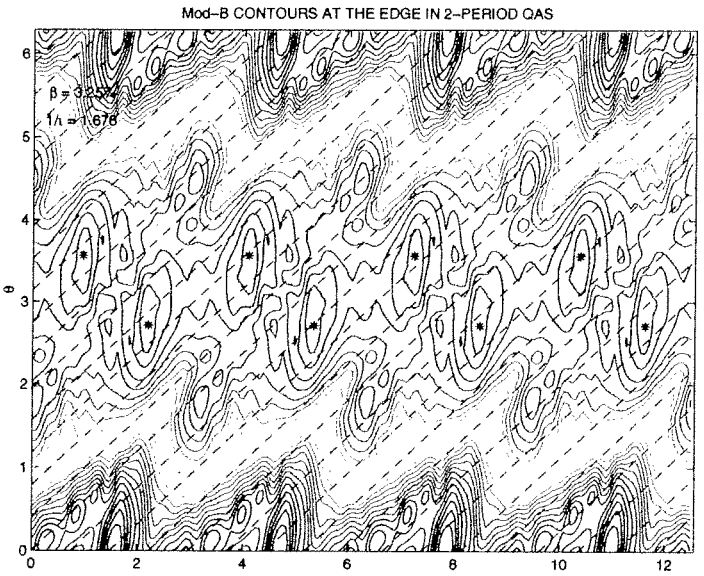

Fig. 6. The mod-B distribution near the plasma edge. The dashed lines are B-field traces. $*$ indicates B-maxima location.

7 Effect of a Vertical Magnetic Field

To counter the outward radial displacement of the plasma column at finite β, a vertical magnetic field (VF) can be used. A set of circular coils of radius $R_{VF} = 20m$ from the major axis and $Z_{VF} = \pm 4m$ from the midplane with a current $I_{VF}/I_{HF} = 0.2$, where the current in the main helical is $I_{HF} = 16.2MA$, is applied. In Fig. 12, we present the

plasma-vacuum interface boundary for the cases with and without VF when $\beta \simeq 3.25\%$ and a self consistent BC included. The magnitude of the VF roughly restores the plasma shape and position of the vacuum state obtained in the absence of the VF. However, examining the B^2 spectrum profiles reveals that a significant mirror contribution ($m = 0, n = 1$) is introduced (Fig. 13) which could spoil confinement properties.

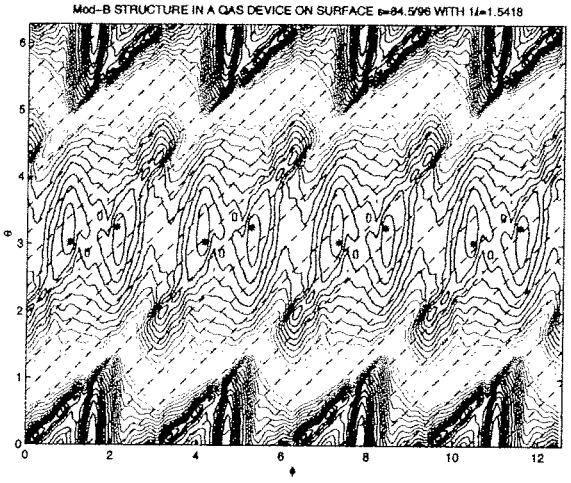

Fig. 7. The mod-B distribution at $\beta = 3.78\%$ on an unwrapped flux surfaces with $s = 84.5/96$.

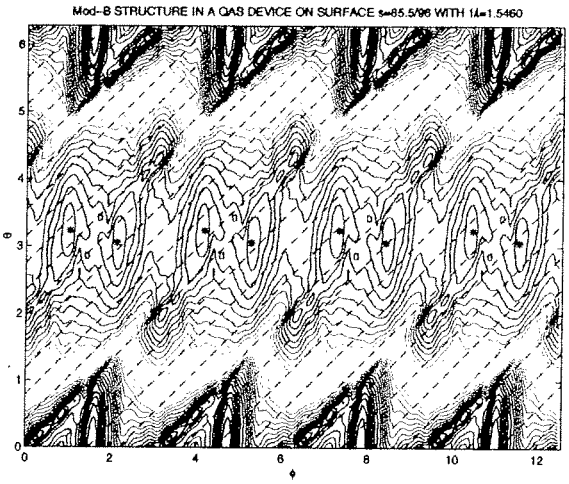

Fig. 8. The mod-B distribution at $\beta = 3.78\%$ on an unwrapped flux surfaces with $s = 85.5/96$.

8 Conclusions

We have investigated the impact of the bootstrap current in the collisionless $1/\nu$ regime on the free boundary MHD equilibrium and stability properties of a compact 2-field period QAS reactor. The mod-B spectrum of the system under inverstigation is dominated by the $m = 1, n = 0$ component. Finite β causes the plasma column to shift outwards closer to the coils. Including a self consistent BC at the same β value causes the plasma to become more elongated in the vertically and horizontally up-down symmetric cross sections, but only marginally displacing the column further outward radially.

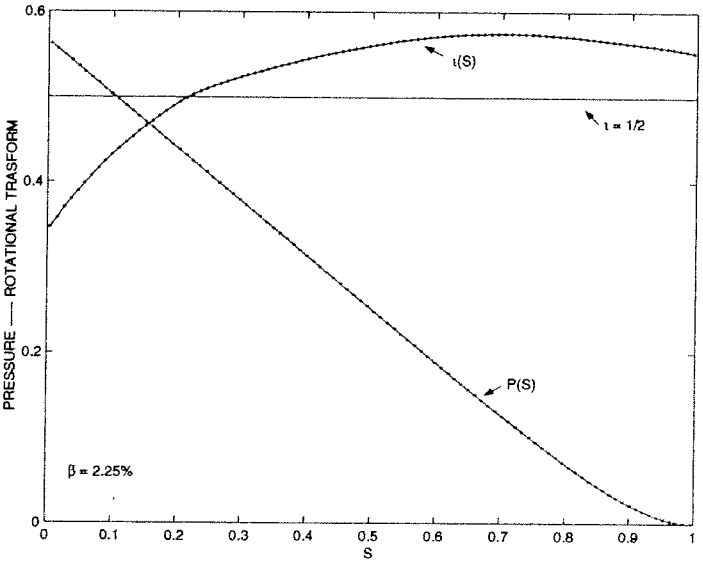

Fig. 9. The pressure and ι profiles at $\beta = 2.25\%$.

The horizontally elongated cross section becomes distorted acquiring a bomblet shape. The application of a vertical magnetic field with currents in the VF coils 20% of the main HF coils can restore the plasma shape and column position to the vacuum state in the absence of VF, but tends to introduce a significant mirror component in the mod-B spectrum. The application of resonant detuning to resolve singularities in the BC near rational magnetic surfaces is very effective for $\beta < 3\%$. At higher β values, the amplitude of the detuning parameter Δ^2 must be increased to achieve converged BC profiles, but with indications that it suppresses the magnitude of the BC towards the edge of the plasma. Discontinuities in the BC profile for $\beta > 3\%$ can be attributed to jumps in the location of the B-maxima on adjacent flux surfaces. The BC causes the rotational transform profile to exceed the critical value $\iota = 1/2$ at $\beta \simeq 2\%$ and provides the free energy to destabilise an external $m/n = 2/1$ global kink mode.

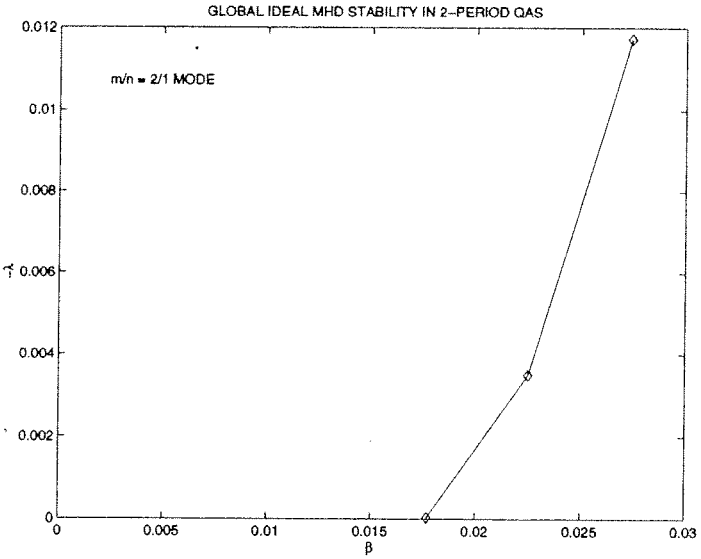

Fig. 10. The unstable eigenvalue as a function of β.

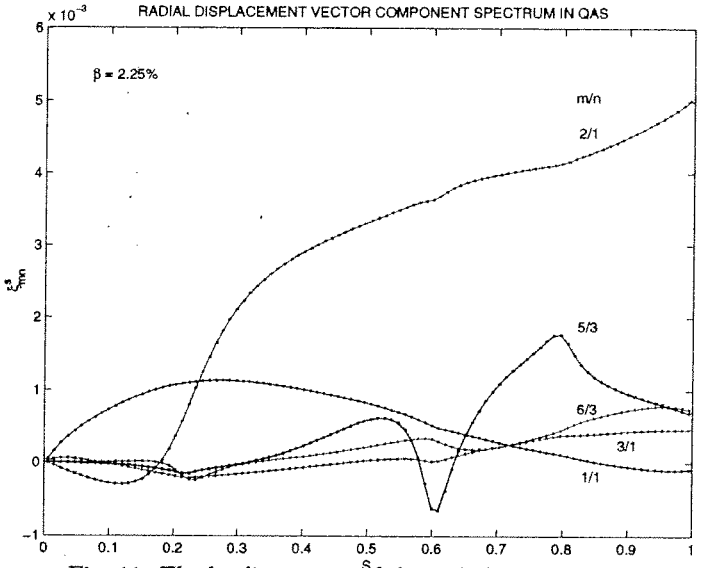

Fig. 11. The leading terms of the radial component of the radial displacement vector profiles at $\beta = 2.25\%$.

Acknowledgments This research was partially sponsored by the Fonds National Suisse de la Recherche Scientifique, Euratom and INTAS. We thank Dr. S.P. Hirshman for the use of the VMEC code. The numerical calculations were primarily performed on a NEC/SX5 platform at the Centro Svizzero di Calcolo Scientifico, Manno, Switzerland.

References

[1] J. Nührenberg et al., Proc. Joint Varenna-Lausanne Int. Workshop on Theory of Fusion Plasmas, Editrice Compositori, Bologna (1994).

[2] P.R. Garabedian, Phys. Plasmas **3**, 2483 (1996).

[3] A.H. Boozer, Phys. Fluids **23**, 904 (1980).

[4] G.H. Neilson et al., Phys. Plasmas **7**, 1911 (2000).

[5] S. Okamura et al., J. Plasma Fusion Res. **1**, 164 (1998).

[6] M. Isobe et al., 28th EPS Conference on Contr. Fusion and Plasma Phys., Funchal, Portugal, ECA Vol. **25A**, 761 (2001).

[7] W.A. Cooper, S. Ferrando i Margalet, S.J. Allfrey et al. Plasma Phys. Controlled Fusion **44** B357 (2002).

[8] J.L. Johnson, K. Ichiguchi, Y. Nakamura, M. Okamoto, M. Wakatani, N. Nakajima, Phys. Plasmas **6**, 2513 (1999).

[9] G.Y. Fu et al., submitted to Fusion Science and Technology (2003).

[10] S.P. Hirshman et al., Comput. Physics Commun. **43**, 143 (1986).

[11] D.V. Anderson et al., Int. J. Supercomp. Appl. **1**, 34 (1990).

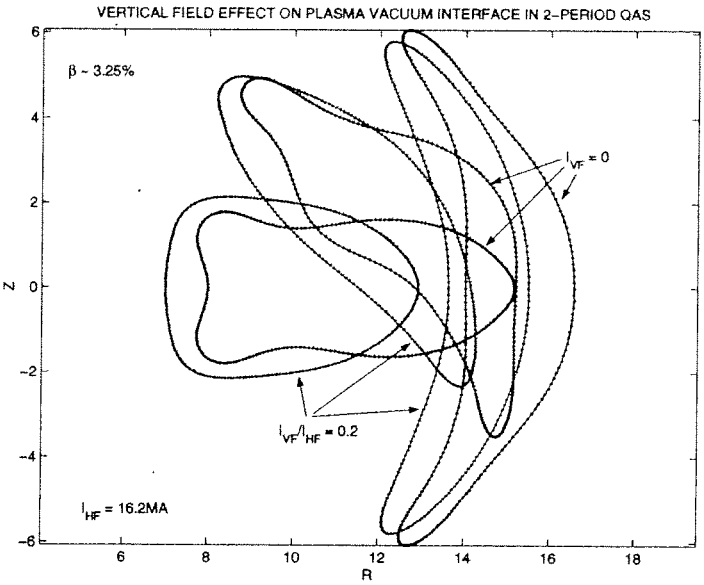

Fig. 12. The plasma-vacuum interface boundary shapes at 3 cross sections within half a period in a QAS reactor with and without vertical field.

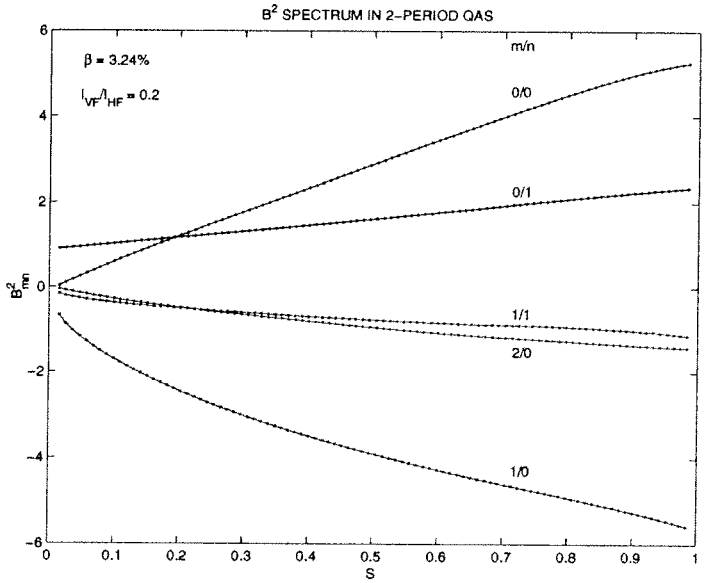

Fig. 13. The leading components of the B^2 spectrum profiles at $\beta = 2.25\%$.

Bootstrap Current and Quasi-symmetry in Reactor-Size Stellarators

S. Ferrando i Margalet[1], W.A. Cooper[1], S.J. Allfrey[1], P. Popovitch[1], M.Yu. Isaev[2]

[1] *Centre D Recherches en Physique des Plasmas, Association Euratom-Confédération Suisse, Ecole Polytechnique Fédérale de Lausanne, PPB, 1015 Lausanne, Switzerland*

[2] *Russian Research Centre "Kurchatov Institute", 123182, Moscow, Russia*

1.Introduction

Recently, the possibility of quasi-symmetric stellarators as efficient fusion reactors has been thoroughly studied [1, 8, 2, 3, 6, 7]. The main idea is to optimize the helical configuration in order to obtain a magnetic topography independent of a certain symmetry coordinate. Among them there are three main categories: the quasi-axisymmetric (QAS), the quasi-helically symmetric (QHS) and the quasi-isodynamic. The three types have different symmetry coordinate and different magnetic topography. Particles following magnetic field lines in magnetically confined plasmas become trapped when their momentum is insufficient to overcome a certain value of the magnetic field strength. The interaction between these particles and the passing ones gives rise to the so-called bootstrap current (BC). In tokamaks, with their axisymmetry, and in quasi-axisymmetric devices, particles become trapped mostly in toroidal wells and the resulting BC contributes to increase the rotational transform. Configurations with more helical symmetry, instead, will have their trapped particles confined preferably in helical wells which effect will be to decrease the transform.

QAS and QHS systems have different symmetry and magnetic topography of the magnetic surfaces, thus, the resulting BC is very different as well as it is its effect on the rotational transform ι and stability.

In this paper we will restrict our calculations to a 3-period QAS based on the NCSX (Princeton, USA) and 4-period QHS based on the HSX (Wisconsin, USA) systems, both extrapolated to reactor size. In order to expect a certain configuration to be candidate to fusion reactor, the β should be able to be increased up to values 5%. BC calculations for increasing values of β have been undertaken for both configurations. The relevance of the asymmetric modes is also studied for both systems. Finally the implications of increasing β and non-symmetric modes in the stability of the system are discussed.

2.Calculation of the bootstrap current

MHD momentum balance equation method

Our aim is to describe a method to calculate BC applicable to any reactor-like configuration. The calculations are undertaken consistently with the equilibrium in a similar way as the one followed in [3]. Being at reactor level it is interesting to be working with relatively high β, i.e. $\beta \approx 5\%$. Also high temperatures and densities are required, hence, it is not unreasonable to consider ions and electrons to be both in the collision-less regime and same temperature (conditions assumed in our calculations).

The BC is evaluated numerically in the collision-less 1/v regime for a pure electron and ion plasma with $T_i = T_e$, as described in [9] and implemented in the TERPSICHORE code [5]. VMEC equilibria [4] are computed iteratively until the BC converges. Departing from a zero current specification, the equilibrium is calculated together with an associated, but inconsistent, BC. This BC is included in the specification of the next equilibrium. Convergence is achieved when the BC from a particular equilibrium differs from the previous one within a given tolerance (in our case: $(\mu_0 j_B(i) - \mu_0 j_B(i-1)) \leq 0.02[HA/m] \approx 16kA$). A nearly parabolic pressure profile

$$P(s) = P_0[(1-s) - 0.1(1-s^{10})]$$

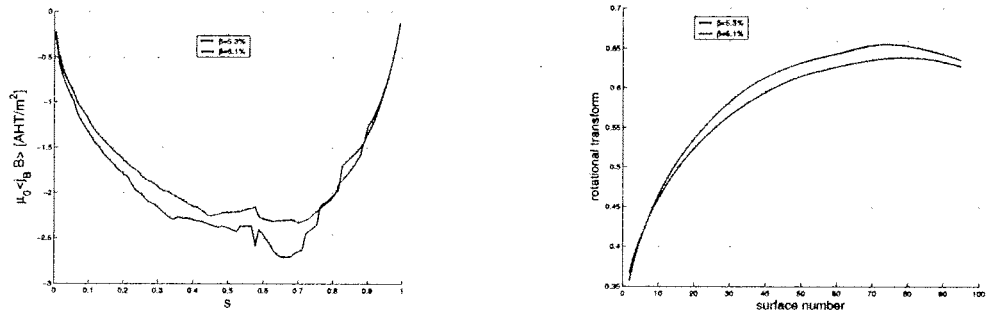

Figure 1: **Left: BC profiles for β of 5.3% and 6.1% respectively. Right: ι profiles cs. β. It can be seen how ι approaches dangerously the value 2/3, when $\beta = 6.1\%$.**

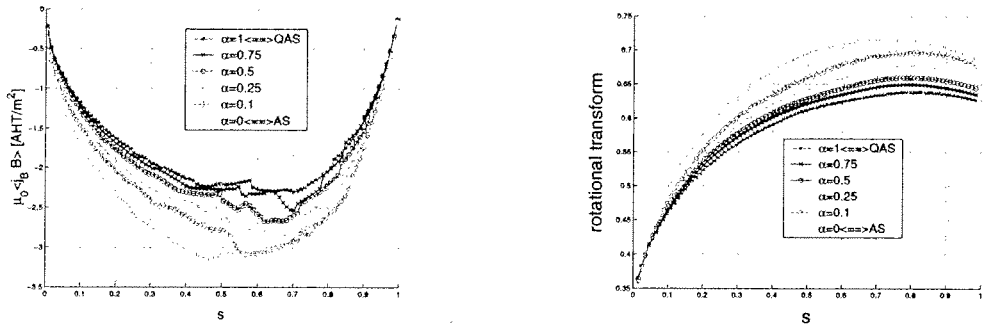

Figure 2: **Left: BC profiles for different values of α., Right: ι profiles for different values of α. Configurations with $\alpha \leq 0.25$ cross the m/m=3/2 rational surface, becoming unstable.**

which provides a vanishing pressure gradient at the edge, is prescribed. The density profile is taken to be:

$$N(s) = (1 - s^{\ell})^q$$

in particular with $\ell = 2$ and $q = 1$. These values can be varied along with the pressure profile.
The TERPSICHORE code, in which this BC calculations are embedded, transforms the VMEC output into Boozer coordinates, in which the magnetic field lines are straight. This allows to have a very useful picture of the topography of the magnetic field surfaces. Hence, once a BC-consistent equilibrium is obtained with its final consequent iota profile, we can have an intuitive picture of any magnetic surface and the magnetic field lines wrapped around it, clarifying the behavior of the trapped and passing particles.

3.Results

QAS

For the 3-period QAS considered convergence was achieved up to $\beta = 6.1\%$. It can be seen that increasing β increases also the transform (Fig.1 left and right). For the limiting value of $\beta = 6.1\%$, ι approached dangerously the m/n=3/2 rational surface weakly destabilizing the configuration (Fig.1 (right)). The system was completely stable for $\beta = 5.3\%$.
In order to study the effect of the symmetrization of the configuration a parameter α has been included in the calculations. α ranges from 0 to 1 and multiplies the non-axisymmetric terms, i.e. $n \neq 0$, so $\alpha = 1$ would give the actual quasi-axisymmetric geometry, while $\alpha = 0$ would be a completely axisymmetric one. The BC profiles (Fig.2 (left)), the ι profiles (Fig.2 (right)) and the total BC (Fig.4 (left)) are represented for different values of α. The total difference between the BC values considering and not considering the non-symmetric modes is $\approx 30\%$. In fact when only the 25% of the non-symmetric modes is taken into account the decrease in the total BC is of $\approx 13\%$.

We can visualize the effect of the non-symmetric modes on the magnetic topography in Fig. 3. It can be seen that the consideration of the $n \neq 0$ terms indeed disrupts the

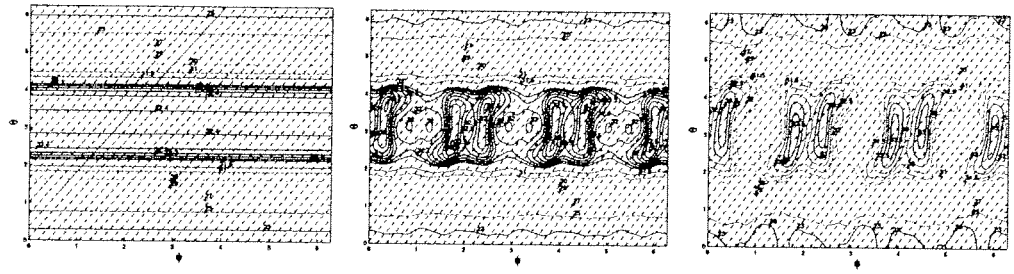

Figure 3: **Left:Mod-B contours for $\alpha = 0$, i.e., completely AS, with $\beta = 5.3\%$ and s=0.5. Center: Mod-B contours for $\alpha = 0.25$, i.e., the 25% contribution of the non-axisymmetric modes is considered, with $\beta = 5.3\%$ and s=0.5. Right: Mod-B contours for $\alpha = 1.0$, i.e., completely QAS, with $\beta = 5.3\%$ and s=0.5.**

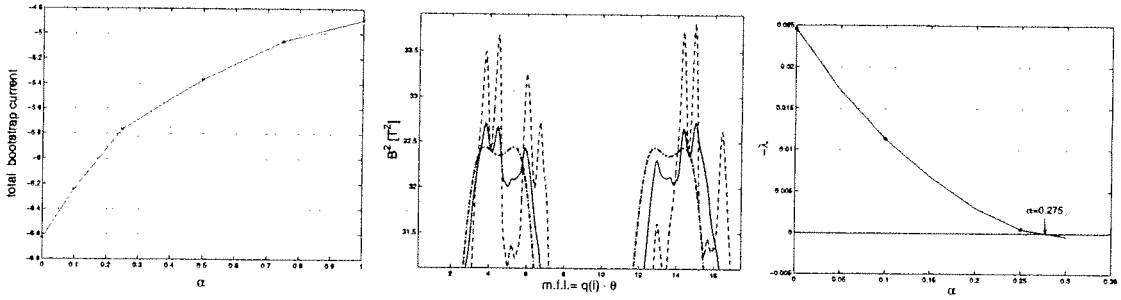

Figure 4: **Left: Surface integrated values of BC vs. α. Half of the total difference between $\alpha = 0 and 1$ is already achieved when $\alpha - 0.25$. Center: Mod-B felt by particles following for $\alpha = 0, 0.25, 1, \beta = 5.3\%$ and s=0.5. The effect of the asymmetry is manifested in the materialization of local maxima within the high field region. Right: Rayleigh quotient vs. α. The stability limit appears right after $\alpha = 0.25$, when iota crosses the m/n=3/2 rational surface (see Fig.2 (right)).**

axisymmetric topography. Local maxima are created enabling particles to get trapped in local helical wells. This is better represented in Fig.4 (center) where the mod-B felt by a particle following a magnetic field line is sketched. In the figure the maxima of mod-B are represented, where the effect of the asymmetry is relevant to the BC. When the trapping involves a long excursion of the trapped particle along the magnetic field line, it is called toroidal.This gives a BC which enhances the rotational transform. When it is within a short range in the evolution of the magnetic field line the trapping is called helical and the result is a contribution to the BC in the direction which decreases ι.

The figure shows the magnetic field strength felt by a particle for the cases of complete axisymmetry ($\alpha = 0$, dot-dash line), full quasi-axisymmetry($\alpha = 1$, dashed line) and finally when only the 25% of the magnitude of each non-axisymmmetric mode is considered $\alpha = 0.25$, solid line). Local maxima and mimima arise in the high field region and behave like helical traps, in which previously free or toroidally trapped particles may become now helically trapped. Producing an opposite BC which decreases the total current.
These results show that any model considering only axisymmetric terms could possibly overestimate the total BC. This turns out to be relevant in stability studies. In fact Fig.4 (right) shows that, for $\beta = 5.3\%$, the $\alpha = 0$ case is unstable and only becomes stable for $\alpha > 0.25$, when ι falls below 2/3 (see Fig.2(right)).

QHS

A QHS configuration is designed to reduce the effect of toroidicity in the geometry. The magnetic field spectrum is dominated by the Bmm components. The magnetic field seen by a particle following a magnetic field line is rapidly varying. The consequent magnetic wells imply a helical trapping of particles in which the trapped particle excursion along the field line before bouncing back is very short. This kind of trapping produces a BC

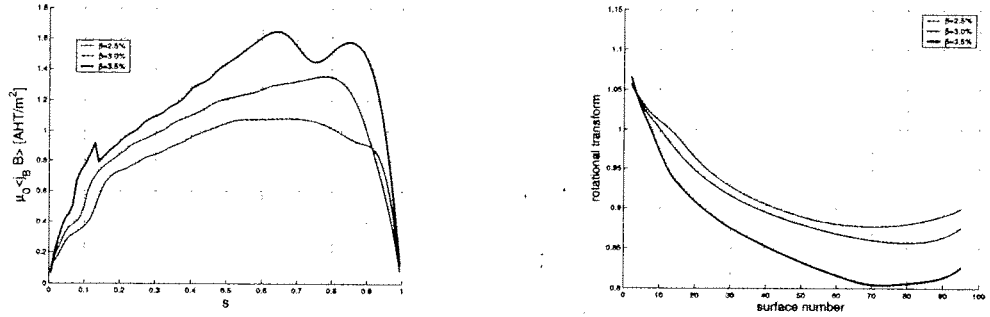

Figure 5: **Left: BC profiles for β =2.5, 3 and 3.5%. Calculations with higher values of β failed to converge. Right: ι profiles for β =2.5, 3 and 3.5%.**

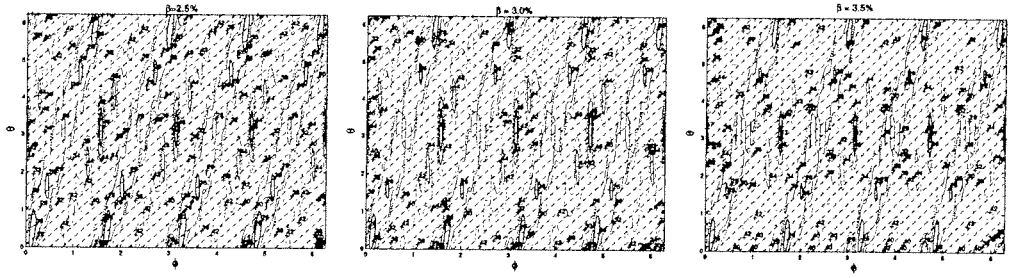

Figure 6: **Left: Mod-B contours for β = 2.5%, surface number 82/96 (approximately s=0.85). Center: Mod-B contours for β = 3.0%, for the same magnetic surface. Right: Mod-B contours for β = 3.5%, for the same magnetic surface.**

in the direction that decreases the rotational transform. The main results obtained for this configuration are the following: The BC obtained is rather large and in the opposite direction from the QAS case. As a consequence the alteration of the equilibrium due to the effect on the transform makes this configuration more difficult to converge. In particular, when increasing β, the convergence becomes more and more difficult, and it has shown to be unreachable for $\beta \geq 3.5\%$.

Figs.5 (left and right), show the strong dependence of the BC and ι on β. When β is increased from 2.5 to 3.5% the BC rises 30% in absolute value. As a result the ι profile decreases substantially. However, as can be seen in Figs.6 (left, center and right) for the surface 82/96 (approximately s=0.85) in this case the change in BC is not so much due to the change of the mod-B topography in which the only difference is the slight increase of the local maxima. Insteadm seems to be mostly a result of the fact that a particle close to the barely trapped limit would encounter a higher density of mod-B maxima when β increases. Hence, more helical traps.

To study the relevance of the non-helically symmetric terms, the modes with $B_{mn}, m \neq n$ have been multiplied as in the previous case, by a parameter α. When $\alpha = 1$ the configuration has the actual QHS geometry while when $\alpha = 0$ the resulting spectrum is purely helically symmetric. Our method failed to converge for $\alpha < 0.25$ (Figs.7 left and right). However, there is not a significant change in BC due to the non-symmetric modes: the difference in total BC between $\alpha = 0.25$ and $\alpha = 1.0$ is $\approx 1\%$. The resulting effect on ι is also very small.

No stability results have been obtained for QHS at this time.

4.Conclusions

We have investigated the BC in the $1/\nu$ regime in quasiaxisymmetric and quasi helically symmetric systems. In the 3-period QAS, the BC increases ι while in the QHS it decreases it. The method used enables us to visualize the relationship between the BC obtained, its effect on the ι-profile and the way particles would get trapped due to the magnetic

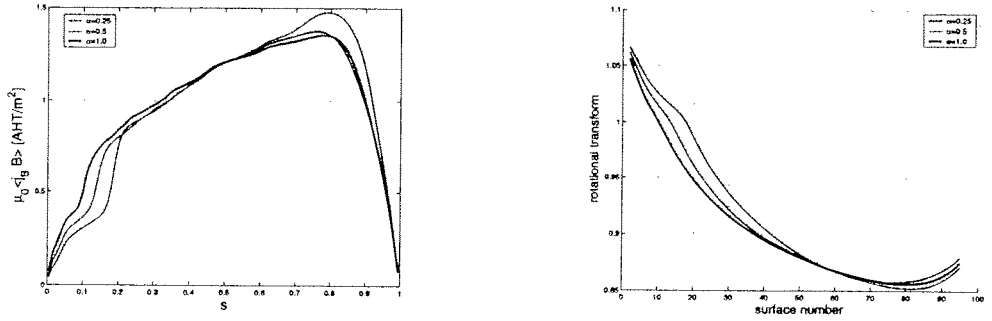

Figure 7: **Left: BC profiles for α =0.25, 0.5 and 1.0 (completely QHS). Calculations failed to converge for $\alpha < 0.25$. Right: ι profiles for α =0.25, 0.5 and 1.0.**

geometry. It is shown how toroidally and helically trapped particles would give BC in opposite directions and how they combine to give the total BC.
In QAS, convergence has been achieved for $\beta \leq 6.1\%$ with fixed boundary VMEC equilibrium. In QHS, our calculations failed to converge for $\beta > 3.5\%$. In the lattercase, an increase of the absolute value of the BC of nearly 40% at s=0.85 is observed. The mod-B maps, show that this is mainly due not to any major change in the magnetic topography but on the change in the ι, since a particle following a magnetic field line would encounter a greater amount of helical traps.
The relevance of the non-symmetric modes in the calculation of the BC has also been studied for both quasi-symmetric systems. In the 3-period QAS the non-symmetric modes seem to be indeed relevant since, when not included in the calculations, the BC drops by 27%. In fact if only 25% of the magnitud of each non-symmetric mode is considered, the change in the magnetic topography of the magnetic surface is enough to alter the trapping of particles in such a way that the BC decreases 13%. For the QHS, on the other hand, the supression of the non-symmetric modes does not seem to affect significantly the BC. However, convergence could not be achieved when less than 25% of the magnitude of each of these modes was considered.
Finally the stability of the systems has also been investigated. In the 3-period QAS, the configuration was stable for $\beta \approx 5\%$, but when β was pushed up to around 6% the increase in the BC also incremented ι which approached the m/n=3/2 rational surface, making the equilibrium weakly unstable. As for the symmetry studies, the consideration of only symmetric modes when $\beta = 5.3\%$, would give an unstable equilibrium. Nevertheless, even if only slightly more than 25% of the nagnitude of each non-symmetric mode was considered, the effect on the magnetic geometry, the trapping of particles, and its consequent decrease of the BC, was sufficient to decrease the ι below the m/n=3/2 threshold, stabilizing the configuration.
Stability calculations for the QHS system will be addressed in the future.

5. Acknowledgments

This work was partly supported by the Swiss National Science Foundation. We thank Dr. S. P. Hirshman for the use of the VMEC code. We also aknowledge Dr. M.C. Zarnstorff for the NCSX input and Dr. J.N. Talmadge for the HSX input.

References

[1] P.R. Garabedian, Proc. 13th Int. Stellarator Workshop (Canberra 2002)
[2] D.T. Anderson, Fusion Technology 27, 273 (1995)
[3] M. Isobe, S. Okamura, et al., Proc. 28th EPS Conference on Contr. Fusion and Plasma Phys., Funchal, 18-22, June 2001

[4] S.P. Hirshman, U. Schwenn and J. Nührenberg, J. Comput. Phys. 87, 396 (1989)
[5] D.V. Anderson, W.A. Cooper, R. Gruber, S. Merazzi and U. Schwenn, The International Journal of Supercomputer Applications 4, 34 (1990)
[6] A. Reiman,G. Fu, et al, Plasma Phys. Control. Fusion 41 (December 1999) B273-B283
[7] S. Okamura, K. Matsuda, et al., Nuclear Fusion 41, num.12, 1865 (2001)
[8] Paul Garabedian, Long-Poe Ku, Physics of Plasma 6, num 3, 645 (1999)
[9] Johnson et al,Phys. Plasmas 6 2513 (1999)

3D Full Wave Propagation Code for Cold Plasma

P.Popovich, W.A.Cooper, L.Villard

Centre de Recherches en Physique des Plasmas,
Association EURATOM - Confédération Suisse, EPFL, 1015 Lausanne, Switzerland

A new solver for low-frequency electromagnetic (E/M) perturbations in general three-dimensional plasma configurations is presented (LEMan). The studies of the E/M wave propagation in stellarators in Alfvén and ICRF ranges of frequency demonstrate a large variety of possible approximations, plasma models and approaches to solve the propagation problem [1, 2, 3]. The interest in this research is explained by the need for tools for the analysis of the radio-frequency heating, stability and current-drive in stellarators. We are developing a code for the numerical simulation of small E/M perturbations excited with antenna currents in 3D inhomogeneous plasma configurations. As required for the low-frequency propagation studies, no assumption is made on the wavelength relative to the characteristic gradient lengths and the problem is solved globally. The frequency range is limited by the numerical resolution because the discretization should allow for at least several grid points per wavelength, which is hard to afford at high frequency.

Rather than using the traditional field formulation of the Maxwell equation

$$\nabla \times \nabla \times \vec{E} - k_0^2 \hat{\epsilon} \cdot \vec{E} = i k_0 \frac{4\pi}{c} \vec{j}_{ext}, \qquad k_0 = \omega/c \tag{1}$$

we reformulate it in terms of the E/M potentials $(\vec{A}, \phi)$:

$$\begin{array}{l} \vec{B} = \nabla \times \vec{A} \\ \vec{E} = -\nabla\phi + i k_0 \vec{A} \end{array} \qquad \left\{ \begin{array}{rcl} \nabla^2 \vec{A} + k_0^2 \hat{\epsilon} \cdot \vec{A} + i k_0 \hat{\epsilon} \cdot \nabla\phi & = & -\frac{4\pi}{c} \vec{j}_{ext} \\ \nabla \cdot (\hat{\epsilon} \cdot \nabla\phi) - i k_0 \nabla \cdot (\hat{\epsilon} \cdot \vec{A}) & = & -4\pi\rho_{ext} \end{array} \right. \tag{2}$$

The reason for using the potential formulation is the so-called numerical pollution effect. It has been shown that the discretization of the Maxwell equation applying standard finite element method introduces unphysical solutions that are very hard to "filter" from the physical solution [4]. In the case of cubic finite elements these spurious solutions appear even at arbitrarily fine mesh. The potential formulation (2), on the contrary, guarantees a pollution-free numerical solution.

To solve the equations (2) we first multiply them by arbitrary test functions $\vec{F}, G$ correspondingly and then integrate over the calculation domain including the vacuum region. The results presented here are obtained with the fixed-boundary version of the code, without the vacuum, but the formulation of the wave problem is general and does not change for a free-boundary case. The integration in the plasma is done over magnetic surfaces and in vacuum – over pseudo-surfaces. The first pseudo-surface coincides with the plasma-vacuum interface, and the last one – with the wall. After integration by parts only the first-order derivatives of $\vec{A}$ and ϕ remain:

$$\left\{ \begin{array}{l} \int_\Omega dV \left[-(\nabla \times \vec{F}) \cdot (\nabla \times \vec{A}) - (\nabla \cdot \vec{F})(\nabla \cdot \vec{A}) + k_0^2 \vec{F} \cdot (\hat{\epsilon} \cdot \vec{A}) + i k_0 \vec{F} \cdot (\hat{\epsilon} \cdot \nabla\phi) \right] \\ \qquad + \int_{\delta\Omega} \vec{dS} \cdot \left[\vec{F} \times \nabla \times \vec{A} + \vec{F} (\nabla \cdot \vec{A}) \right] = -\frac{4\pi}{c} \int_\Omega dV \vec{F} \cdot \vec{j}_{ext} \\ \int_\Omega dV \left[\nabla G \cdot (\hat{\epsilon} \cdot \nabla\phi) - i k_0 \nabla G \cdot (\hat{\epsilon} \cdot \vec{A}) \right] + \int_{\delta\Omega} \vec{dS} \cdot \left[i k_0 G \, \hat{\epsilon} \cdot \vec{A} - G \, \hat{\epsilon} \cdot \nabla\phi \right] \\ \qquad = -4\pi \int_\Omega dV G \rho_{ext}, \end{array} \right. \tag{3}$$

The wave-plasma interaction is described here by the dielectric tensor $\hat{\epsilon}$. At present, we have implemented the full cold plasma model [5]. Despite being simple, this model, however, can give an insight on the structure of the Alfvén continuum and discrete modes and simulate mode conversion effects (conversion to the short wavelength oscillations appearing at the Alfvén resonant surfaces). The antenna is modeled by specifying the volume density of external helical divergence-free currents $\vec{j}_{ext}$ and charges ρ_{ext} in the vacuum or inside the plasma.

The magnetic equilibrium configuration is first produced with the VMEC code [6]. It is then transformed to the Boozer magnetic coordinates [7] using the TERPSICHORE code [8]. LEMan has an interface to TERPSICHORE and uses Boozer angles as poloidal and toroidal coordinates.

To simplify the boundary conditions and the analysis of the results, we have chosen an orthogonal basis for the vector potential representation, formed by the directions of the magnetic field, the normal to the surface, and the binormal direction. These three components of $\vec{A}$ and the scalar potential ϕ constitute the actual unknowns of the equation. With this choice, the boundary conditions on the conducting shell take a very simple form:

$$A_b(s=1,\theta,\phi)=0, \qquad A_{||}(s=1,\theta,\phi)=0, \qquad \phi(s=1,\theta,\phi)=0 \tag{4}$$

The discretization of the equation is made by decomposing these unknown functions over a finite set of one-dimensional functions: Fourier decomposition in poloidal and toroidal angles and finite elements in the radial direction. Standard linear "hat" functions and Hermite cubics have been implemented.

$$A_k(s,\theta,\phi)=\sum_{r,m,n} A_k^{rmn}\psi_r(s)e^{i(m\theta+n\phi)}, \qquad \phi(s,\theta,\phi)=\sum_{r,m,n}\phi^{rmn}\psi_r(s)e^{i(m\theta+n\phi)} \tag{5}$$

where $k=(n,b,||)$, θ,ϕ are the Boozer angles, $\psi_r(s)$ are the radial basis functions (this representation is slightly more complicated for Hermite cubic basis functions, A_k and ψ_r being two-component vectors, but we do not show it here for simplicity). The same decomposition is applied to the test functions $\vec{F},G$. Using Fourier transform in both angles may be particularly efficient in the case of Alfvén waves because the condition for the Alfvén resonance and mode conversion is satisfied on the magnetic surfaces [9], at least in axisymmetric configurations, and the number of Fourier modes needed to describe the solution may be relatively small in this case.

The discretized equation should be satisfied with any arbitrary functions $\vec{F},G$, so this condition gives us the final equation in a simple matrix form:

$$\hat{M}\cdot A = J \tag{6}$$

where $A=\{A_k^{rmn}\}$ and J is the antenna contribution. Each element of the matrix $\hat{M}$ is a volume integral:

$$M_{rr'kk'}^{mm'nn'}=\int_\Omega dV\left[\sum_{i,j=0}^{3}C_{ijkk'}(s,\theta,\phi)\frac{\partial}{\partial u_i}\left(\psi_r(s)e^{i(m\theta+n\phi)}\right)\frac{\partial}{\partial u_j}\left(\psi_{r'}(s)e^{i(m'\theta+n'\phi)}\right)\right] \tag{7}$$

where $u_1=s, u_2=\theta, u_3=\phi$, while the label $\dfrac{\partial}{\partial u_0}$ implies that no derivative is performed.

The analytical expressions for the coefficients $C_{ijkk'}(s,\theta,\phi)$ in general 3D geometry are composed of a very large number of terms (thousands!) and are hard to write down

even for the cold plasma model. In order to simplify the coding and avoid mistakes when expanding the expressions, we use symbolic manipulation software (Mathematica). It generates a Fortran code that can then be directly used for the numerical evaluation of the terms. The coefficients $C_{ijkk'}(s,\theta,\phi)$ store the information about the equilibrium quantities (metric elements, magnetic field) and the dielectric tensor, but do not depend on the perturbations. This fact is used to optimize the evaluation of the volume integrals. Instead of calculating the integrals (7) directly in real space, the equilibrium coefficients $C_{ijkk'}(s,\theta,\phi)$ are first Fourier-transformed in the poloidal and toroidal angles. This limits the number of 3D integrals to be evaluated by the number of equilibrium Fourier modes, which is usually much smaller than the number of all possible combinations of the perturbed mode pairs $(m,n),(m',n')$. The integrals (7) are thus reduced to 1D radial integrals of the sums of Fourier coefficients. Only one equilibrium Fourier mode contributes to the sum for each given combination (m,n,m',n'). This method is considerably faster than evaluation of the volume integrals in real space for each perturbation mode. For example, for a simple 3D case tested a run for one antenna frequency takes only 90 seconds instead of 10 hours for the algorithm with real-space integral evaluation.

Specific loop optimisation for the vector processor computing (on the NEC SX5) has helped to further reduce the matrix construction time. The largest fraction of the runtime (typically, 80% for a 3D configuration) is thus spent on the sparse matrix solution. One can hope then that improving the plasma model may not lead to a dramatic increase in runtime. Typically, the time needed for a 2D run is about 10-100 seconds: a fully 3D configuration with 100 radial nodes and 100 Fourier (m,n) harmonics requires about 1000 seconds at 3-3.5 Gflops and about 10 Gb of memory.

A power balance is used for the self-consistency check of the numerical solution. It can be easily verified that the variational form (3) exactly corresponds to the energy conservation law, except for the terms with $\nabla\cdot\vec{A}$. While the *exact* solution of the Eq. (2) can be divergence-free under certain conditions, the *numerical* solution can only converge to it, but the value of the divergence is finite. Indeed, a combination of the two equations in (2) results in the Laplace equation for the $\nabla\cdot\vec{A}$: $\nabla^2(\nabla\cdot\vec{A})=0$ (for the divergence-free antenna currents). Therefore, if the divergence is imposed to be zero on the domain boundary, the *exact* solution is divergence-free everywhere. The value of $\nabla\cdot\vec{A}$ and its contribution to the power balance can thus be used as an estimate for the convergence of the numerical results. Another two values used for the convergence check are relative averaged local and global power balances.

$$\begin{aligned}
\delta_d &= \int\limits_\Omega \left|\nabla\vec{A}\right| dV V^{1/3} \Big/ \int\limits_\Omega \left|\vec{A}\right| dV \\
\delta_l &= \int\limits_0^1 \left|P_{plasma}(s) - P_{ant}(s) - iS_{flux}(s)\right| ds \\
\delta_g &= \left(P_{plasma}(1) - P_{ant}(1)\right)/P_{plasma}(1)
\end{aligned} \tag{8}$$

Here, $P_{plasma}(s)$ is the total power absorbed in the plasma between the magnetic axis and the magnetic flux surface labeled s, $P_{ant}(s)$ is the power coupled in the antenna inside this surface and iS_{flux} is the inward power flux through this surface. The real part of these variables corresponds to the reactive power, the imaginary part is the resistive power. As the classical cold plasma dielectric tensor does not include resistivity, we model it by introducing a small imaginary part in the frequency.

In Fig.1, a convergence study is presented for a typical 2D configuration (2D is chosen to be able to go further in the number of radial grid points and Fourier modes).

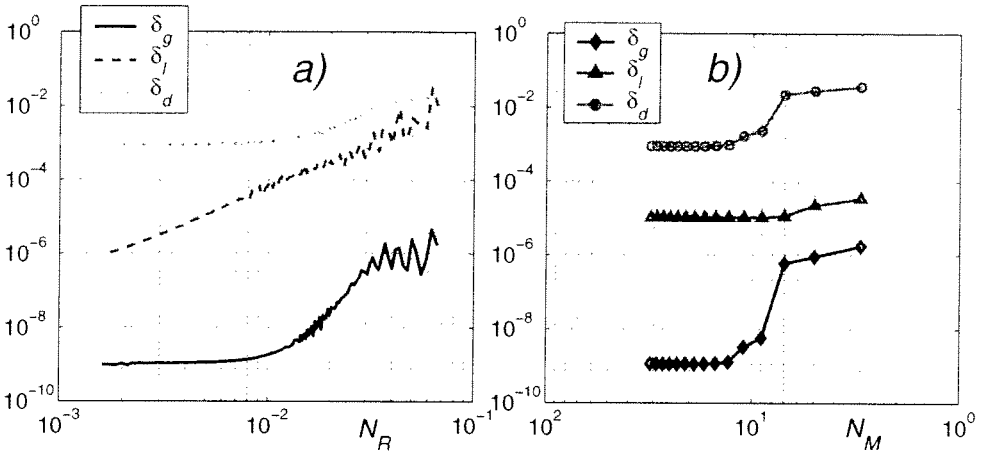

Figure 1. *a) Convergence with the radial mesh size N_R, the number of Fourier harmonics fixed (N_M = 21), b) Convergence with the number of Fourier modes N_M, the radial mesh size fixed (N_M = 200).*

These results are obtained using Hermite cubics for radial discretization with a uniform grid. The mesh size less than 30 nodes does not allow to resolve the short wavelength oscillations near the Alfvén resonant surface. Increasing the N_R, δ_d and δ_g values converge very fast up to a radial mesh size of 100 points and then do not improve much because of the finite number of Fourier modes N_M and the imperfections of the underlying numerical equilibrium. The plot on the right shows exponential convergence with Fourier mode numbers up to 13 and then, again, finite limit due to the equilibrium imprecision and fixed N_R. In all the cases analysed, the global energy balance was much easier to satisfy than either δ_d or δ_l even with very poor numerical resolution.

The code has been previously tested in 1D configurations (comparisons with analytical results) and in 2D (comparison with a 2D LION code [10]). The mode spectrum of a cylinder is completely reproduced in the large aspect ratio limit. The results for an axisymmetric configuration are in a good agreement with the LION results [11]. 1D and 2D results are relatively easy to interpret. Unfortunately, in 3D geometry, the results become very hard to analyse because of the 3D coupling between virtually all the harmonics. As a result of coupling of both poloidal and toroidal modes, the spectrum differs significantly from the corresponding picture in the cylindrical geometry and the modes are impossible to decouple (hence, the eigenmodes are immersed in the Alfvén continuum and are hard to identify). Before applying the code to a fully 3D 2-period QAS stellarator [12], we have studied simpler configurations. In order to get a qualitative idea of the mode structure and main couplings we have first studied different limits of the QAS configuration with the same q per period profile. Starting from a straight cylinder (approximated by a torus with $R/a = 100$) and adding different equilibrium modes we could separate the coupling mechanisms and limit the number of coupled harmonics. This makes it easier to identify the main perturbation modes in these relatively simple cases and compare them with the cylindrical branches. For example, a frequency scan for a cylinder with elliptical cross section (dominant equilibrium modes $(m,n) = (0,0), (\pm 2,0)$) shows that the coupling between even poloidal harmonics results in the formation of the gaps near the crossing of the corresponding circular cylinder branches of the continuum. As a result of the coupling a global eigenmode appear in the gap, the Ellipticity Induced Alfvén eigenmode (EAE). Because of the symmetry of the equilibrium, even and odd poloidal modes are decoupled. Similarly, a mirror-like configuration (large aspect ratio 'bumpy' torus)

with dominant $(0,0)$, $(0,\pm 60)$ has a gap formed due to the coupling between different toroidal harmonics, multiples of 60. Gap modes, the Mirror Induced Eigenmodes (MAE), are again present in the plasma response scan. The same holds for the equilibrium with helical symmetry. Helical equilibria are a very convenient way of testing the 3D structure of the code, having the advantage of allowing simple analysis of the results. On the one hand, it is a fully 3D configuration that is solved in a square box of Fourier components, without any assumption on the symmetry of the equilibrium. On the other hand, this helical symmetry allows us to select only a few coupled modes and compare them with the corresponding cylindrical branches.

The next configuration is an axisymmetric equilibrium, a torus of the same aspect ratio as QAS and the same q profile (all the $n \neq 0$ modes in the QAS equilibrium are forced to 0). A frequency scan for this configuration shows several gaps and eigenmodes. The easiest to identify are the eigenmodes due to the coupling between modes (-2,2) and (-6,2) (c); (-3,2) and (-5,2) (d); (-4,2) and (-3,2) (e). Even distant poloidal modes $m = -2$ and $m = -6$ are coupled because of the strong shaping of the QAS.

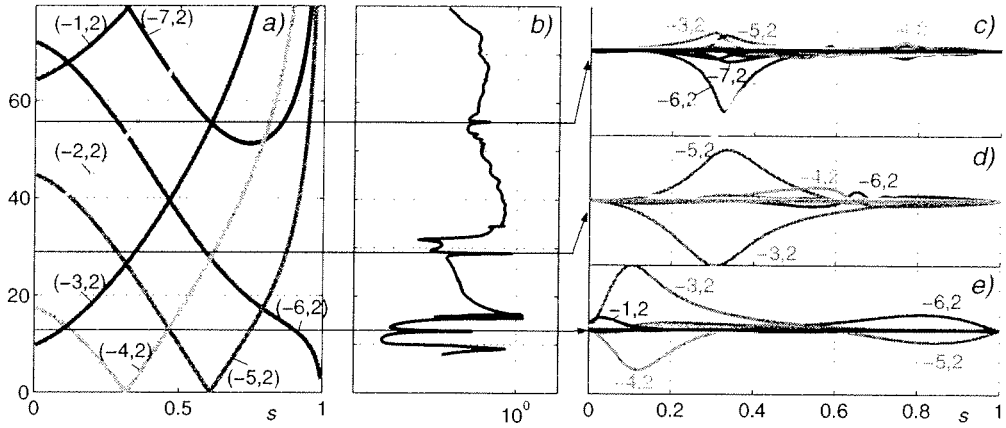

Figure 2. *a) Mode structure for a cylinder with the same q profile as the QAS, b) normalized plasma response. c)-e) wavefields ($A_{||}$,[a.u]) at f=56.0, 28.9 and 12.8 kHz.*

And, finally, a frequency scan has been performed for the fully 3D QAS configuration (aspect ratio of approximately 3.5). As expected, the mode coupling structure becomes very complicated and hard to analyse. All the gaps become 'closed', e.g. they are immersed in the Alfvén continuum of the other branches. However, a comparison with the cylindrical continuum can still be helpful (Fig.3). For example, we see that the cylindrical branches (-9,4) and (-7,2) cross at s 0.7, which is close to the surface of maximum amplitude of these modes at f=48.5kHz in the QAS. The (-3,2) mode appears to have an Alfvén resonance surface at s=0.55, close to its cylindrical position.

Summary and conclusions

A new 3D solver for E/M wave propagation has been developed and applied to 2D and 3D configurations. The full wave equation in terms of E/M potentials is solved in a general numerical 3D equilibrium, provided with the VMEC and TERPSICHORE codes. The Boozer coordinate system is used. Discretization is done with Fourier decomposition in poloidal and toroidal angles and finite elements (linear and cubic) radially. A power balance is used for the self-consistency check of the results. It also provides a measure

for the convergence estimate. The relative errors in the power balance and the $\nabla \cdot \vec{A}$ contribution decrease with the radial mesh size and the number of Fourier harmonics. The global power balance is very easily satisfied ($\delta_g = 10^{-6}$) even at very low numerical resolutions. Due to the optimised algorithm of equilibrium coefficient evaluation in Fourier space, the matrix construction time is largely decreased. This makes it possible to perform a frequency scan for fully 3D configurations in a reasonable time. Several spectra have been analysed for various equilibria with different symmetries and effects of different types of mode coupling presented (gap formations, presence of discrete eigenmodes). The analysis in the 3D QAS stellarator geometry is complicated by the coupling of m and n modes, but a comparison with the corresponding cylindrical branches still proves to be useful and helps to distinguish the main modes and mode conversion surfaces.

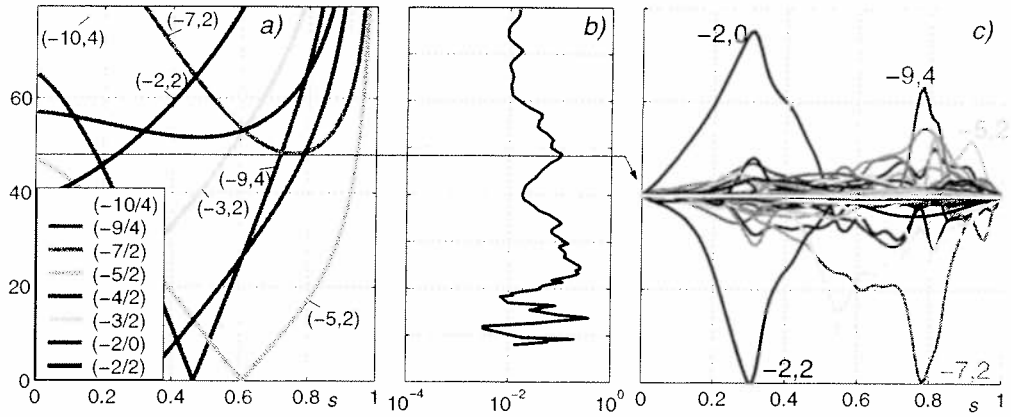

Figure 3. *a) Mode structure for a cylinder with the same q profile as the QAS, b) normalized plasma response, c) wavefields ($A_{||}$,[a.u]) at f=48.5 kHz. Only dominant Fourier harmonics are shown.*

Acknowledgement: We thank Dr. S.P.Hirshman for the use of the VMEC code. This work was partly supported by the Swiss National Science Foundation. Some of the calculations were performed on the NEC-SX5 platform at the Centro Svizzero di Calcolo Scientifico, Switzerland.

References

[1] E. F. Jaeger, L. A. Berry, E. D'Azevedo, D. B. Batchelor, M. D. Carter, and K. F. White, Phys. of Plasma 9(5) (2002) 1873
[2] V.Vdovin, T.Watari, A.Fukuyama, Proc.ICPP 96 (Nagoya 1996),1070; NIFS-469 L.
[3] C. Nührenberg, Phys. of Plasmas 6(1), 137 (1999)
[4] A. Jaun, K. Appert, J. Vaclavik, L. Villard, Comp. Phys. Comm. 92, 153 (1995)
[5] T.H.Stix, "The theory of plasma waves", McGraw-Hill Book, London, 1962.
[6] S.P. Hirshman, U. Schwenn and J. Nührenberg, J. Comput. Phys. 87, 396 (1989)
[7] A. Boozer, Phys. Fluids 23(5), 904 (1980)
[8] D.V. Anderson, W.A. Cooper, R. Gruber, S. Merazzi and U. Schwenn, The International Journal of Supercomputer Applications 4, 34 (1990)
[9] E. Tennfors, Plasma Phys. Contr. Fus. 28 (1986) 1483
[10] L. Villard, K. Appert, R. Gruber, J. Vaclavik, Comput. Phys. Reports 4 (1986) 95
[11] P.Popovich, W.A.Cooper, L.Villard, Proc. 29th EPS, Montreux, 2002
[12] P.R.Garabedian, Phys. Plasmas 3, 2483 (1996)